Published in final edited form as:
Bone. 2014 July ; 64: 173–182. doi:10.1016/j.bone.2014.04.011.

Fabrication, vascularization and osteogenic properties of a novel synthetic biomimetic induced membrane for the treatment of large bone defects

Liling Ren[#a,b], **Yunqing Kang**[#a], **Christopher Browne**[a], **Julius Bishop**[a], and **Yunzhi Yang**[a,c,*]

[a]Department of Orthopaedic Surgery, Stanford University, 300 Pasteur Drive, Stanford, CA 94305,USA

[b]School of Stomatology, Lanzhou University, 199 Donggang West Road, Lanzhou, Gansu 730000, China

[c]Department of Materials Science and Engineering, Stanford University, 300 Pasteur Drive, Stanford, CA 94305,USA

[#] These authors contributed equally to this work.

Abstract

The induced membrane has been widely used in the treatment of large bone defects but continues to be limited by a relatively lengthy healing process and a requisite two stage surgical procedure. Here we report the development and characterization of a synthetic biomimetic induced membrane (BIM) consisting of an inner highly pre-vascularized cell sheet and an outer osteogenic layer using cell sheet engineering. The pre-vascularized inner layer was formed by seeding human umbilical vein endothelial cells (HUVECs) on a cell sheet comprised of a layer of undifferentiated human bone marrow-derived mesenchymal stem cells (hMSCs). The outer osteogenic layer was formed by inducing osteogenic differentiation of hMSCs. *In vitro* results indicated the undifferentiated hMSCs cell sheet facilitated the alignment of HUVECs and significantly promoted the formation of vascular-like networks. Furthermore, seeded HUVECs rearranged the extracellular matrix produced by hMSCs sheet. After subcutaneously implantation, the composite constructs showed rapid vascularization and anastomosis with the host vascular system, forming functional blood vessels *in vivo*. Osteogenic potential of the BIM was evidenced by immunohistochemistry staining of osteocalcin, tartrate-resistant acid phosphatase (TRAP) staining, and alizarin red staining. In summary, the synthetic BIM showed rapid vascularization, significant anastomoses, and osteogenic potential *in vivo*. This synthetic BIM has the potential for treatment of large bone defects in the absence of infection.

[*]Corresponding author: Department of Orthopaedic Surgery Stanford University 300 Pasteur Drive Edwards R155 Stanford, CA 94305 Tel: 650-723-0772 Fax: 650-724-5401 ypyang@stanford.edu.

Keywords

Vascularization; Induced membrane; Cell sheet; HUVEC; hMSC

1. Introduction

The treatment of large bone defects caused by trauma or infection remains a substantial clinical challenge in modern orthopedics. Currently available treatments mainly include vascularized bone transfer [1], cancellous autografting [2], and bone transport [3]. Most recently a two-stage induced membrane technique pioneered by Masquelet and colleagues has received extensive attention [4, 5]. This technique involves the temporary implantation of a polymethyl methacrylate (PMMA) cement spacer into the bony defect which induces the formation of a bioactive membrane. 4 to 8 weeks after cement spacer implantation, the spacer is removed and a cancellous autograft is placed into the membrane. This technique has shown great promise in the management of large bone defects with case reports of successful treatment [4, 6, 7], even greater than 20 cm [8]. Several mechanisms of action are thought to facilitate bone healing in these difficult situations. The presence of the membrane itself compartmentalizes the bone graft, separating it from the surrounding muscle. Previous research has demonstrated that this compartmentalization of bone defects improves bone healing and limits graft resorption [9]. In addition, pluripotent stem cells are present in the membrane along with various growth factors such as vascular endothelial growth factor (VEGF) and bone morphogenetic protein-2 (BMP-2) [10], which are known to be important in fracture healing. Studies have also demonstrated that the membrane is well vascularized and a large number of vessels are present in the fibrous inner layer [11, 12]. These studies suggest that the induced membrane plays a role in osteogenesis as well as vascularization of the bone graft [10, 11].

However, there are some limitations using the induced membrane technique for bone regeneration. Patients have to undergo at least two surgical procedures to implant the PMMA cement spacers and then remove them in addition to any additional procedures required to treat frequently associated soft tissue injuries. The temporary implantation of the PMMA does not guarantee the induction of a robust and appropriately proportioned membrane, and the biologic viability of the membrane appears to degrade over time, peaking 4 weeks after PMMA spacer implantation [10, 13]. One alternative approach to addressing these limitations is to use tissue engineering techniques to create a synthetic bioactive membrane that mimics the structure of an induced membrane. The synthetic membrane could contain and compartmentalize an autogenous or synthetic bone graft to optimize healing. Theoretically, this synthetic membrane could facilitate single-step reconstruction of large bone defects when combined with appropriate internal fixation and autogenous bone graft or synthetic bone scaffold [14]. Successful development of such a synthetic membrane has the potential to decrease the number of procedures required for the reconstruction of large bone defects while optimizing the biologic microenvironment at the fracture site and accelerating healing. Other synthetic membranes fabricated from bioresorbable polylactide [14], collagen barrier [15] or polylactide [16] have been reported for use in reconstruction of segmental bone defects. However, these synthetic membranes

lack both the multiple layered structures and the osteo and angiogenic capacity of a biologically induced membrane.

A novel cell sheet engineering technique developed by Okano and colleagues has proved effective for engineering tissues such as cornea, skin, myocardium, and mucous membrane [17-19], and has also been used to create an osteogenic cell sheet for bone tissue [20-22]. More recently, the pre-vascularization of cell sheet-based constructs has been proposed as a way to circumvent vascularization of 3D thick grafts [23]. Therefore, cell sheet engineering technique has the potential to create a complex 3D synthetic biomimetic induced membrane (BIM).

The purpose of this study is to determine the feasibility of using a cell sheet engineering technique to fabricate a BIM with a similar biological profile to the biologically induced membrane. We first produced a pre-vascularized inner layer by seeding human umbilical vein endothelial cells (HUVECs) on an undifferentiated human bone marrow-derived mesenchymal stem cells (hMSCs) sheet, and then an osteogenic outer layer by inducing the osteogenic differentiation of hMSCs. These two cell sheet layers were wrapped together to form a BIM with similar structural configuration to a biologically induced membrane (Fig. 1). We hypothesized that this pre-vascularized BIM would rapidly anastomose with host vasculature and demonstrate potential osteogenic properties. To this end we prepared a pre-vascularized BIM and characterized its *in vitro* pre-vascularization abilities and *in vivo* functional vascularization in the subcutaneous site of mouse. At the same time, we characterized the osteogenic potential of this BIM.

2. Materials and methods

2.1. Cell culture

A MSCGM™ BulletKit™ was utilized to culture hMSCs. The hMSCs have been shown to express CD105, CD166, CD29 and CD44 more than 90% of the time while expressing CD14, CD34 and CD45 less than 10% of the time (Lonza Inc.). The hMSCs can differentiate into adipogenic, chondrogenic, and osteogenic lineages [24]. The hMSCs were cultured in MSCBM (Lonza), which is a non-differentiating growth medium containing 10% fetal bovine serum (FBS) and 1×glutamine-penicillin-streptomycin (GPS; Invitrogen). HUVECs which continuously express GFP were provided from the late Folkmann laboratory at Children's Hospital (Boston) and cultured in EBM™ (endothelial basal medium) and an EGM™ (endothelial growth media) SingleQuots™ Kit (Lonza). The cell medium was changed every 3 days. Cells below passage 9 were used in all the experiments.

2.2. Production and characterization of pre-vascularized cell sheets

To make the pre-vascularized composite cell sheet, hMSCs were first cultured in a cell culture dish at a cell density of $9\times10^4/cm^2$ in MSCGM medium. After the cells reached confluence, the medium was changed to MSCGM with the addition of 50 μg/ml ascorbic acid and 30 mM glucose to promote the production of extracellular matrix [25]. After 14 days of culture, hMSCs formed a thick cell sheet, referred here as UM.

HUVECs were cultured in EBM-2 and trypsinized after confluence. At day 14 a HUVEC cell suspension was seeded onto the surface of the hMSCs sheet at a cell density of $5\times10^4/cm^2$. After a designated incubation period, the morphology of the cell sheets were observed under a fluorescent microscope and images were captured. We named this HUVEC/hMSC cell sheet layer HUVEC/UM and intended for it to function as the inner pre-vascularized layer. To investigate the patterns of HUVECs pre-vascularized networks on the UM sheet, immunofluorescent staining was performed. Platelet-endothelial cell adhesion molecule (PECAM-1, or CD31), an endothelial-specific adhesion protein and a specific marker of HUVECs, was used to assess HUVECs pre-vascularized networks. After the sheets were washed three times in PBS, a 5% goat serum-PBS buffer solution was used to block the cell sheet samples for 1 hour at room temperature, and then primary antibody mouse anti-human CD31 (89C2, cell signaling technology, dilution 1:3200), mouse anti-human CD90 (550402, BD Bioscience, dilution 1:50), and mouse monocolonal smooth muscle actin (α-SMA, sc-53015, Santa Cruz Biotechnology Inc, dilution 1:200) in 1% BSA-PBS were added into the sample followed by incubation overnight at 4 °C. After washing with PBS, a secondary antibody goat-anti-mouse (Alexa Fluor® 594, 2 μg/ml, Invitrogen) in 1% BSA-PBS was added and incubated in the dark for 1 hour at room temperature. Finally, cell nuclei were counterstained with DAPI (5 μg/ml) for one minute and then extensively washed with PBS. The fluorescent staining was imaged by a confocal microscopy (Zeiss). HUVECs seeded on the well plate were used as a control.

2.3. Production and characterization of mineralized cell sheet

To mimic the structure of a biological induced membrane that contains potential bone-forming cells, an osteogenic hMSCs layer (OM) was synthesized. To obtain this mineralized layer, hMSCs were cultured in osteogenic medium which contained MSCBM supplemented with 10% FBS, 10 nM dexamethasone, 10 mM β-glycerophosphate, 50 μg/ml ascorbic acid and 30 mM glucose. After culturing for 21 days, the mineralization properties were characterized by alizarin red and Von Kossa staining.

2.4. Production and characterization of a 3D BIM construct

To fabricate a 3D BIM construct, a sterilized silicone rubber cylinder was placed on the pre-vascularized HUVEC/UM sheet, and the HUVEC/UM sheet was gently peeled off and rolled onto the rubber cylinder using a cell scraper and a sharpened point forceps (Fig. 1). The silicone rubber was purchased from Rubber Sheet Roll Co. and the diameter was 1.5 mm.

After the cell sheet was rolled onto the rubber, the construct with a multi-layered sheet consisting of HUVEC/UM was placed onto the OM cell sheet. The OM cell sheet was rolled onto the pre-rolled HUVEC/UM sheet. This multi-layered BIM was referred to as OM/HUVEC/UM. As a control, a cell sheet without HUVECs was designed using the same technique, and was referred to as OM/UM. This procedure is illustrated in Fig. 1.

For observing the cross-section of the cell sheets, the HUVEC/UM cell sheets on the rubber cylinder were fixed with 4% paraformaldehyde and immersed in serial sucrose solution from 10% sucrose and 15% sucrose in PBS for 3 h each at room temperature, and then immersed

in 20% sucrose in PBS overnight at 4 °C [26]. Afterwards, the treated samples were frozen in Tissue-Tek O.C.T. compound, and then 7 μm thick sections were cryoprocessed. An immunofluorescent staining was performed on the sections as described above. Also, hematoxylin and eosin (H&E) staining and F-actin staining was performed by conventional methods.

2.5. In vivo implantation

The Administrative Panel on Laboratory Animal Care of Stanford University (APLAC) approved this *in vivo* animal study. The pre-vascularized OM/HUVEC/UM constructs and non-pre-vascsularized OM/UM constructs were prepared as described in Fig. 1 and incubated for 24 h in mixed medium (osteogenic medium:EBM-2 = 1:1) before implantation. The next day, the composite cell sheet constructs were surgically implanted into the subcutaneous tissues of nude mice. In this study male immunodeficient nude mice (6-7 week old, 20-25 g body weight, Charles River Laboratories) were utilized. Two cell sheet constructs (OM/HUVEC/UM and OM/UM) were implanted into two separate subcutaneous dorsal pockets per animal. 25 μg cefazolin/g and 0.1 μg buprenorphine/g mice were administrated, and the mice were put in separate cages after surgery. Each experimental time point and condition was performed with 4 mice. The implants were harvested after 1 and 2 weeks for histological analysis and evaluation of vascularization.

2.6. Histology and Immunohistochemistry assays

After 1 and 2 weeks, the mice were euthanized and the implants were retrieved, fixed in buffered formalin (10%) 24 h, embedded in paraffin, and sliced into 7 μm-thick sections. To evaluate the presence of luminal structures containing red blood cells, conventional H&E staining was carried out on the sections. For immunohistochemistry, sections were de-paraffinized and digested by an antigen retrieval solution, then the sections were blocked by blocking serum (5%) for 30 minutes at room temperature. Rabbit anti-human CD31 antibodies (Clone EP3095 for human microvessel detection; 1:500; Millipore,) were used. Biotinylated goat anti-rabbit secondary antibodies (1:500; Vector Laboratories) and DAB substrate kit (Vector Laboratories) were used followed by hematoxylin counterstaining and permanent mounting. The microvessels formed in the constructs *in vivo* were quantified by evaluation of 8 random view fields (under 40×magnification) of the stained sections that came from 4 individual mice (2 fields per mouse). Luminal structures containing erythrocytes were defined as microvessels. The density of each microvessel was reported as the average number of erythrocyte filled microvessels and expressed as mean values±the standard deviation. The quantitative assay of human lumens containing murine erythrocytes was also performed according to the same method.

2.7. Osteogenic staining

To identify the osteogenic potential within the synthetic BIM, immunohistochemistry staining for osteocalcin, tartrate-resistant acid phosphatase (TRAP) and alizarin red staining were carried out on the 7 μm-thick sections. TRAP staining of osteoclasts was performed using Leukocyte acid phosphate kit (Sigma) with fast red violet according to the

manufacture's instruction. Immunohistochemistry staining of osteoclacin and alizarin red staining were preformed as described above.

2.8. Statistical analysis

All the *in vitro* experimental groups were carried out in triplicate. In the *in vivo* studies, four samples per group were performed. Two-way ANOVA analysis was used to analyze the differences between groups. A p value of less than 0.05 was used to define a significant difference.

3. Results

3.1. Cell morphology on cell sheet

The morphology of the hMSCs sheets after confluence and the cell morphology of HUVECs seeded on the hMSCs sheet were observed under a microscope. After 3 days, hMSCs reached confluence and continued to grow and formed a dense cell sheet. Fig. 2A shows a very dense sheet of hMSCs cultured in undifferentiated medium after 14 days. Observational results indicated that HUVECs started to migrate on the hMSCs cell sheet 2 hours after seeding (data not shown) and continued to form a large number of cell-to-cell alignments after one day. This migration of HUVECs made the hMSCs cell sheet matrix rearrange, leading to the formation of aligned microgrooves at day 3 (Fig. 2B). However, when HUVECs were seeded on a tissue culture plate, this alignment morphology was not observed (Fig. 2C). HUVECs on the hMSCs sheet started to form cords at day 3 (Fig. 2D).

3.2. Immunofluorescent staining and H&E staining

To study the vascularized pattern of HUVECs on the undifferentiated hMSCs sheet *in vitro*, immunofluorescent staining for CD31 expression, a specific endothelial marker for vascularization, was performed. The immunofluorescent images taken at 3, 7 and 14 days revealed a progressive process of lumen morphogenesis. At day 3, HUVECs migrated to induce focal fusion and form small lumens (Fig. 3A). As time increased, more HUVECs elongated and aligned dynamically, resulting in the formation of larger intracellular vacuoles (Fig. 3B). During this initial accumulation of these vacuoles, some of vacuoles started to coalesce. By day 14, larger elongated branches were observed and cells formed intracellular luminal structures (Fig. 3C). However, HUVECs alone cultured on the tissue culture plate did not demonstrate the formation of networks. To observe the cross-section of the pre-vascularized cell sheet, H&E staining on frozen sections was performed. The thickness of the pre-vascularized cell sheet was about 20 μm (Fig. 3G). Immunofluorescent staining for CD31 on frozen sections showed the positive expression of CD31 appeared in the interval of hMSCs nuclei, which suggested that the HUVECs seeded on the hMSCs sheet remodeled the matrix of the hMSCs sheet and embedded into the matrix of the hMSCs sheet after 7 days (Fig. 3H).

To further explore the vascularized patterns, immunofluorescent staining for CD90, which is a surface protein marker of hMSCs, but is not expressed in HUVECs, was performed. Sheet of only hMSCs showed expressions of CD90 in a random pattern. However, hMSCs sheet with seeded HUVECs showed an aligned arrangement of CD90 expression around the

HUVECs in Fig. 4, which was consistent with the observation in Fig. 2c and d. To evaluate if hMSCs have the potential as pericytes when co-culturing with HUVECs in endothelial EBM-2 medium, immunofluorescent staining for α-SMA was performed on the frozen sections. At the early stage (3 and 7 days), there was no obvious expression of α-SMA observed. After 14 days, slight expression of α-SMA was observed, suggesting that hMSCs have little ability to differentiate into myoblasts under the current experimental conditions (Fig. 4).

3.3. Characterization of osteogenic cell sheet

To evaluate if a mineralized hMSCs sheet can be obtained after 21 days of incubation in osteogenic medium as an outer layer of a construct, alizarin red and Von Kossa staining were performed. Results showed extensive mineralized nodule formation due to high calcium deposition (Fig. 5A,B), confirming that hMSCs cultured under these conditions can mineralize to form a mineralized osteoblast cell sheet.

3.4. Characterization of the composite structure before implantation

After detachment from the plates, the sheets could be easily handled with forceps to roll around a rubber cylinder with a diameter of 1.5 mm. Then the composite structure containing a pre-vascularized cell sheet inner layer and osteogenic cell sheet outer layer was continuously cultured in mixed medium (osteogenic medium:EBM-2 = 1:1) for 24 hours (Fig. 6A). H&E staining showed the composite structure consisted of multiple layers of sheets, and the cells in each layer showed the same aligned direction and were embedded into the matrix of each layer (Fig. 6B). F-actin staining was used to evaluate if the cells between two layers could grow together to contact each other. The results indicated that an abundance of actin fibers were present in the cytoplasm of the cells. The cells in different rolled layers can cross and expand to contact each other within and between different layers, in turn facilitating the merging of different cell sheet layers (Fig. 6C). Immunofluorescent staining for CD31 showed that lumen structures appeared among the multilayered constructs (Fig. 6D). This expression of CD31 in the cross-sections clearly demonstrated the lumens formation in the multiple cell sheets.

3.5. Histological identification of vascular networks in implanted construct

To investigate whether the construct's structure with an inner pre-vascularized layer and outer osteogenic layer could support the formation of vascular networks *in vivo*, we surgically implanted the construct into immunodeficient mice (Fig. 7A). Prior to implantation, all the constructs were cultured in a mixture medium for 1 day and OM/UM served as control. At 7 and 14 days after implantation, the composite cell sheet constructs were removed and H&E staining was performed on paraffin sections to show the presence of blood vessels. These blood vessels were identified as lumen containing red blood cells. In OM/UM without HUVECs, few blood vessels were observed at 7 and 14 days (Fig. 7B,D). However, numerous blood vessels containing erythrocytes were observed to be distributed throughout the OM/HUVEC/UM implants (Fig. 7C,E). Our quantification of the microvessel density revealed a statistically significant difference between the OM/HUVEC/UM and OM/UM (Fig. 7G). At 7 days after implantation, the average microvessel

density of the construct with HUVECs was 67±25 vessels/mm^2 compared to 2±6 vessels/mm^2 in those without HUVECs. At 14 days after implantation, the average density in the HUVECs construct was 46±10 vessels/mm^2, compared to 7±8 vessels/mm^2 in the construct without HUVECs. Vessel density within the HUVECs constructs was not significantly different between days 7 and 14.

3.6. Immunohistochemistry identification of functional perfused vessels

To assess the ability of the vessels formed *in vitro* to anastomose with host vasculature and form functional perfused blood vessels *in vivo*, immunohistochemistry staining was carried out using a monoclonal rabbit anti-human CD31. At day 7 and day 14, numerous hCD31-positive blood vessels were present in the OM/HUVEC/UM constructs (Fig. 8B,D). Murine erythrocytes infiltrated the lumen, indicating the formation of functional blood vessels (Fig. 8E). The above result is critical, for it implies that the lumens generated in a pre-vascularized cell sheet succeeded in anastomosing with host vascular system to form functionally perfused blood vessels. In contrast, there were no human blood vessels detected in the implants of OM/UM (Fig. 8A,C).

The density of anastomotic vessels that were hCD31-positive in the intact lumens containing murine erythrocytes was calculated from the immunohistochemistry staining images. In the OM/HUVEC/UM group, the density of lumens was 59±10 vessels/mm^2 after 7 days and 46±4 vessels/mm^2 after 14 days (Fig. 8F). There was no significant difference between these two time points.

3.7. Characterization of osteogenic potential

To determine whether this biomimetic structure has an osteogenic potential in ectopic implantation, immunohistochemistry staining of osteocalcin, TRAP staining for osteoclast, and alizarin red staining for calcium matrix were performed. Immunohistochemistry staining of osteocalcin showed an enhanced concentration of osteocalcin in OM/HUVEC/UM (Fig. 9B) compared to that in the OM/UM construct (Fig. 9A). Sporadic TRAP positive staining were observed in both the OM/HUVEC/UM group and the OM/UM group (Fig. 9C,D), indicating osteoclast activity in the induced membrane [27, 28]. There was robust calcium matrix deposition in OM/HUVEC/UM (Fig. 9F) compared to the construct without HUVECs (Fig. 9E). These results further indicated that the OM/HUVEC/UM has potential for promoting osteogenesis compared to the OM/UM group without pre-vascularization.

4. Discussion

In this study we fabricated a synthetic BIM using a cell sheet engineering technique. We found that the pre-vascularized BIM rapidly anastomosed with host vasculature to form perfused functional vessels, while non-pre-vascularized cell sheets did not. The BIM also demonstrated more osteogenic properties compared to the non-pre-vascularized cell sheets. Our results suggest that the pre-vascularization of the BIM plays an important role in the vascularization, functional anastomosis, and osteogenesis *in vivo*. This BIM could represent an alternative approach to the treatment of a large bone defects.

Previous studies have demonstrated that induced membranes have a highly vascularized inner layer [11], which our synthetic BIM successfully mimicked. We produced a pre-vascularized HUVEC/UM inner layer in the BIM. Our study demonstrated that the undifferentiated hMSCs sheet strongly promoted the network formation of HUVEC, but when endothelial cells were cultured on a tissue culture plate without the hMSCs sheet substrate, HUVECs were randomly distributed (Fig. 2). This implies that the rich ECM derived from hMSCs provides an important organizational cue for cell migration, network formation, and alignment of HUVECs. These processes facilitate pre-vascularization of cell sheets *in vitro* and also explain previously observed cellular interactions between HUVECs and hMSCs in co-cultures [29, 30]. The endothelial cells also re-arranged the matrix of hMSCs sheet in an aligned direction. Our observations are consistent with those of Soucy et al, who thought that endothelial cells could reconstruct or modify the surrounding ECM environment, which is also crucial to the process of tube formation [31]. The interaction between ECM produced by hMSCs and HUVECs may collectively contribute to tube formation, and the further vascularization *in vivo*. Additional research is needed to better understand these complex relationships.

These pre-vascularized networks formed *in vitro* anastomosed with the host vascular system *in vivo* after implantation. The synthetic BIM demonstrated capillary-like structures and indicated the *in vitro*, pre-formed, vascular-like network rapidly integrated with the host vasculature and formed functional blood vessels. This was likely a result of both host vasculature invasion and vascular bed formation [32] as well as host vasculature connecting with the pre-vascularized networks created *in vitro*. It appears that hMSCs play an important role in the process as they have previously been demonstrated to function as pericytes [23, 33]. These perivascular cells can express angiogenic factors [34], which induce host blood vessel invasion and stabilization. Studies have shown that biologically induced membranes produce angiogenic growth factors (VEGF, TGFβ1) and osteoinductive factors (BMP-2) after 4 weeks [10, 35]. However, as our purpose is to develop a BIM and characterize its vascaularization and osteogenesis potential *in vitro* and *in vivo*, we did not investigate whether the BIM secreted growth factors. Studies have reported that endothelial cells secrete BMP-2 and MSCs produce aniogenic factors [36, 37]. The VEGF and other cytokines produced by this BIM may stimulate the host vasculature to infiltrate the construct while simultaneously promoting the anastomosis of pre-formed networks with the host vasculature to form functional perfused blood vessels [38, 39]. In addition to a highly vascularized inner layer, previous studies of induced membranes have identified an outer layer that contains large amounts of collagen bundles parallel to the membrane surface [10]. We mimicked this outer layer by fabricating an osteogenic cell sheet made of differentiated and mineralized hMSCs (osteoblasts-like). Our result demonstrates the osteogenic potential of pre-vascularized BIM. However, there is no quantitative data to indicate a significant difference in the mineralized matrix between these two groups. We have not yet identified the crystal phase of the mineralized matrix or quantified the amount of the mineral matrix *in vivo* versus *in vitro*. We plan to perform these osteogenesis studies in segmental bone defects in the future.

There are several limitations of this BIM in this study. Although the biologic properties of this cell-sheet-engineered BIM are promising, the mechanical properties may not be sufficient for clinical applications. In this study, an inert rubber was used to construct and support the three-dimensional structure. At the same time, utilizing inert rubber allowed us to avoid any biological effects of the supporting material itself. When used clinically, additional support, such as that derived from a bioactive porous bioresorbable polymer or ceramic scaffold may be necessary to address this issue. Furthermore, the synthetic BIM described in this study is intended for reconstruction of a sterile bone defect and not for infection. An appropriate debridement to eradicate infection is still necessary prior to addressing the bone defect. Also, the primary purpose of this study was to develop a novel BIM and characterize its vascularization and osteogenesis. In situ orthotopic studies in bone defects will be necessary to investigate the osteogenesis of this synthetic BIM and learn more about potential clinical efficacy. Moreover, additional qualitative and quantitative studies will be necessary to better understand osteogenesis.

Despite these limitations, the BIM described in this study has the potential to improve the treatment of large bone defects. The BIM could be used to encapsulate and augment autogenous bone graft in a large defect while allowing patient and surgeon to avoid the additional surgery required for the placement of a PMMA spacer to induce a membrane. Additional studies are indicated to expand the clinical applications of this BIM.

5. Conclusion

We fabricated a synthetic BIM that has the potential to improve the treatment of critical bone defects. The synthetic BIM with an inner pre-vascularized layer and outer osteogenic layer demonstrated rapid vascularization, functional anastomosis properties, and osteogenic potential *in vivo*. Additional research is needed to evaluate the efficacy of this membrane in enhancing the healing and reconstruction of critical bone defects.

Acknowledgments

This work was supported by grants from the following agencies: NIH R01AR057837 (NIAMS), NIH R01DE021468 (NIDCR), DOD W81XWH-10-1-0966 (PRORP), Wallace H. Coulter Foundation, National Natural Science Foundation of China (No. 81170938, 81300860), and Chinese

Fundamental Research Funds for the Central Universities (lzujbky-2013-173).

References

[1]. Pelissier P, Casoli V, Demiri E, Martin D, Baudet J. Soleus-fibula free transfer in lower limb reconstruction. Plast Reconstr Surg. 2000; 105:567–73. [PubMed: 10697162]

[2]. Keating JF, Simpson AH, Robinson CM. The management of fractures with bone loss. J Bone Joint Surg Br. 2005; 87:142–50. [PubMed: 15736731]

[3]. Cattaneo R, Catagni M, Johnson EE. The treatment of infected nonunions and segmental defects of the tibia by the methods of Ilizarov. Clin Orthop Relat Res. 1992; 143:52.

[4]. Masquelet AC. Muscle reconstruction in reconstructive surgery: soft tissue repair and long bone reconstruction. Langenbecks Arch Surg. 2003; 388:344–6. [PubMed: 13680234]

[5]. Retzepi M, Donos N. Guided Bone Regeneration: biological principle and therapeutic applications. Clin Oral Implants Res. 2010; 21:567–76. [PubMed: 20666785]

[6]. Masquelet AC, Fitoussi F, Begue T, Muller GP. [Reconstruction of the long bones by the induced membrane and spongy autograft]. Ann Chir Plast Esthet. 2000; 45:346–53. [PubMed: 10929461]

[7]. Accadbled F, Mazeau P, Chotel F, Cottalorda J, Sales de Gauzy J, Kohler R. Induced-membrane femur reconstruction after resection of bone malignancies: three cases of massive graft resorption in children. Orthop Traumatol Surg Res. 2013; 99:479–83. [PubMed: 23608487]

[8]. Taylor BC, French BG, Fowler TT, Russell J, Poka A. Induced membrane technique for reconstruction to manage bone loss. J Am Acad Orthop Surg. 2012; 20:142–50. [PubMed: 22382286]

[9]. Klaue K, Knothe U, Anton C, Pfluger DH, Stoddart M, Masquelet AC, Perren SM. Bone regeneration in long-bone defects: tissue compartmentalisation? In vivo study on bone defects in sheep. Injury. 2009; 40(Suppl 4):S95–102. [PubMed: 19895960]

[10]. Pelissier P, Masquelet AC, Bareille R, Pelissier SM, Amedee J. Induced membranes secrete growth factors including vascular and osteoinductive factors and could stimulate bone regeneration. J Orthop Res. 2004; 22:73–9. [PubMed: 14656662]

[11]. Woon CY, Chong KW, Wong MK. Induced membranes--a staged technique of bone-grafting for segmental bone loss: a report of two cases and a literature review. J Bone Joint Surg Am. 2010; 92:196–201. [PubMed: 20048113]

[12]. Cuthbert RJ, Churchman SM, Tan HB, McGonagle D, Jones E, Giannoudis PV. Induced periosteum a complex cellular scaffold for the treatment of large bone defects. Bone. 2013; 57:484–92. [PubMed: 23954755]

[13]. Pelissier P, Martin D, Baudet J, Lepreux S, Masquelet AC. Behaviour of cancellous bone graft placed in induced membranes. Br J Plast Surg. 2002; 55:596–8. [PubMed: 12529009]

[14]. Meinig RP. Clinical use of resorbable polymeric membranes in the treatment of bone defects. Orthop Clin North Am. 2010; 41:39–47. table of contents. [PubMed: 19931051]

[15]. Mundell RD, Mooney MP, Siegel MI, Losken A. Osseous guided tissue regeneration using a collagen barrier membrane. J Oral Maxillofac Surg. 1993; 51:1004–12. [PubMed: 8355090]

[16]. Sverzut CE, Faria PE, Magdalena CM, Trivellato AE, Mello-Filho FV, Paccola CA, Gogolewski S, Salata LA. Reconstruction of mandibular segmental defects using the guided-bone regeneration technique with polylactide membranes and/or autogenous bone graft: a preliminary study on the influence of membrane permeability. J Oral Maxillofac Surg. 2008; 66:647–56. [PubMed: 18355588]

[17]. Yang J, Yamato M, Shimizu T, Sekine H, Ohashi K, Kanzaki M, Ohki T, Nishida K, Okano T. Reconstruction of functional tissues with cell sheet engineering. Biomaterials. 2007; 28:5033–43. [PubMed: 17761277]

[18]. Okano T, Yamada N, Sakai H, Sakurai Y. A novel recovery system for cultured cells using plasma-treated polystyrene dishes grafted with poly(N-isopropylacrylamide). J Biomed Mater Res. 1993; 27:1243–51. [PubMed: 8245039]

[19]. Kushida A, Yamato M, Konno C, Kikuchi A, Sakurai Y, Okano T. Decrease in culture temperature releases monolayer endothelial cell sheets together with deposited fibronectin matrix from temperature-responsive culture surfaces. J Biomed Mater Res. 1999; 45:355–62. [PubMed: 10321708]

[20]. Ma D, Ren L, Liu Y, Chen F, Zhang J, Xue Z, Mao T. Engineering scaffold-free bone tissue using bone marrow stromal cell sheets. J Orthop Res. 2010; 28:697–702. [PubMed: 19890976]

[21]. Pirraco RP, Obokata H, Iwata T, Marques AP, Tsuneda S, Yamato M, Reis RL, Okano T. Development of osteogenic cell sheets for bone tissue engineering applications. Tissue Eng Part A. 2011; 17:1507–15. [PubMed: 21275832]

[22]. Ma D, Yao H, Tian W, Chen F, Liu Y, Mao T, Ren L. Enhancing bone formation by transplantation of a scaffold-free tissue-engineered periosteum in a rabbit model. Clin Oral Implants Res. 2011; 22:1193–9. [PubMed: 21303418]

[23]. Mendes LF, Pirraco RP, Szymczyk W, Frias AM, Santos TC, Reis RL, Marques AP. Perivascular-like cells contribute to the stability of the vascular network of osteogenic tissue formed from cell sheet-based constructs. PLoS One. 2012; 7:e41051. [PubMed: 22829909]

[24]. Melero-Martin JM, De Obaldia ME, Kang SY, Khan ZA, Yuan L, Oettgen P, Bischoff J. Engineering robust and functional vascular networks in vivo with human adult and cord blood-derived progenitor cells. Circ Res. 2008; 103:194–202. [PubMed: 18556575]

[25]. Villars F, Bordenave L, Bareille R, Amedee J. Effect of human endothelial cells on human bone marrow stromal cell phenotype: role of VEGF? J Cell Biochem. 2000; 79:672–85. [PubMed: 10996857]

[26]. Sasagawa T, Shimizu T, Sekiya S, Haraguchi Y, Yamato M, Sawa Y, Okano T. Design of prevascularized three-dimensional cell-dense tissues using a cell sheet stacking manipulation technology. Biomaterials. 2010; 31:1646–54. [PubMed: 19962187]

[27]. Rooker SM, Liu B, Helms JA. Role of Wnt signaling in the biology of the periodontium. Developmental Dynamics. 2010; 239:140–147. [PubMed: 19530172]

[28]. James IE, Dodds RA, Lee-Rykaczewski E, Eichman CF, Connor JR, Hart TK, Maleeff BE, Lackman RD, Gowen M. Purification and characterization of fully functional human osteoclast precursors. J Bone Miner Res. 1996; 11:1608–18. [PubMed: 8915768]

[29]. Villars F, Guillotin B, Amedee T, Dutoya S, Bordenave L, Bareille R, Amedee J. Effect of HUVEC on human osteoprogenitor cell differentiation needs heterotypic gap junction communication. Am J Physiol Cell Physiol. 2002; 282:C775–85. [PubMed: 11880266]

[30]. Guillotin B, Bourget C, Remy-Zolgadri M, Bareille R, Fernandez P, Conrad V, Amedee-Vilamitjana J. Human primary endothelial cells stimulate human osteoprogenitor cell differentiation. Cell Physiol Biochem. 2004; 14:325–32. [PubMed: 15319536]

[31]. Soucy PA, Romer LH. Endothelial cell adhesion, signaling, and morphogenesis in fibroblast-derived matrix. Matrix Biol. 2009; 28:273–83. [PubMed: 19375504]

[32]. Melero-Martin JM, De Obaldia ME, Allen P, Dudley AC, Klagsbrun M, Bischoff J. Host myeloid cells are necessary for creating bioengineered human vascular networks in vivo. Tissue Eng Part A. 2010; 16:2457–66. [PubMed: 20218762]

[33]. Caplan AI. All MSCs are pericytes? Cell Stem Cell. 2008; 3:229–30. [PubMed: 18786406]

[34]. Jain RK. Molecular regulation of vessel maturation. Nat Med. 2003; 9:685–93. [PubMed: 12778167]

[35]. Deckers MM, van Bezooijen RL, van der Horst G, Hoogendam J, van Der Bent C, Papapoulos SE, Lowik CW. Bone morphogenetic proteins stimulate angiogenesis through osteoblast-derived vascular endothelial growth factor A. Endocrinology. 2002; 143:1545–53. [PubMed: 11897714]

[36]. Wang J, Ye Y, Tian H, Yang S, Jin X, Tong W, Zhang Y. In vitro osteogenesis of human adipose-derived stem cells by coculture with human umbilical vein endothelial cells. Biochem Biophys Res Commun. 2011; 412:143–9. [PubMed: 21806974]

[37]. Grellier M, Bordenave L, Amedee J. Cell-to-cell communication between osteogenic and endothelial lineages: implications for tissue engineering. Trends Biotechnol. 2009; 27:562–71. [PubMed: 19683818]

[38]. Carano RA, Filvaroff EH. Angiogenesis and bone repair. Drug Discov Today. 2003; 8:980–9. [PubMed: 14643161]

[39]. Mayr-Wohlfart U, Waltenberger J, Hausser H, Kessler S, Gunther KP, Dehio C, Puhl W, Brenner RE. Vascular endothelial growth factor stimulates chemotactic migration of primary human osteoblasts. Bone. 2002; 30:472–7. [PubMed: 11882460]

Highlights

- A biomimetic induced membrane (BIM) was developed using cell sheet engineering.
- The BIM consists of an inner pre-vascularized layer and an outer osteogenic layer.
- The BIM demonstrates rapid vascularization and significant anastomoses.
- The BIM shows osteogenic potential *in vivo*.

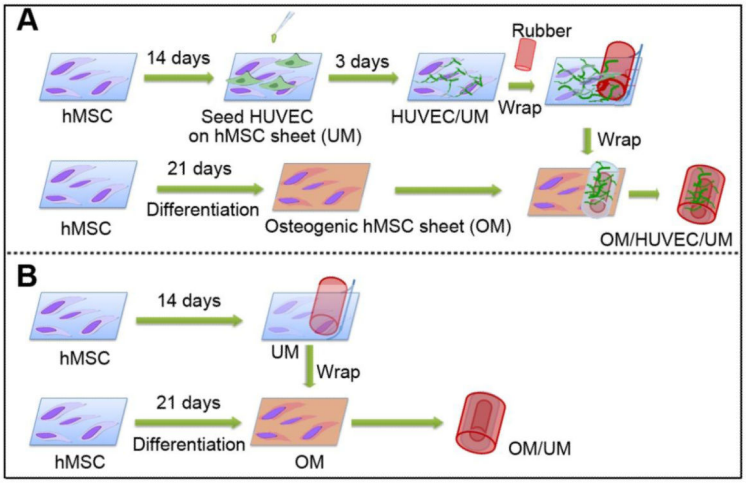

Fig.1.

The schematic of the fabrication of a compound construct OM/HUVEC/UM (A) and OM/UM (B) based on cell sheet engineering.

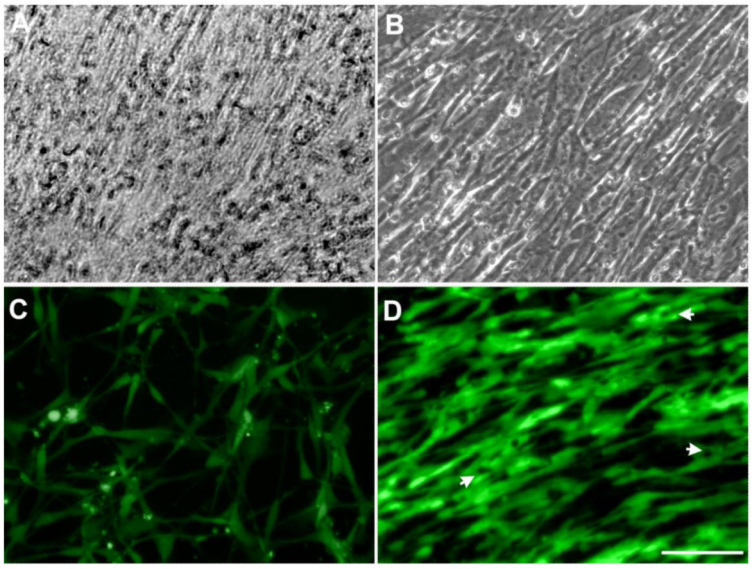

Fig.2.

Light microscopy images of hMSCs cultured in MSCGM for 14 days showing that hMSCs formed a dense cell sheet (A). HUVECs aligned on the hMSCs sheet after 3 days (B). Fluorescent images show that HUVECs cultured on the well-plate display normal cell morphology (C) but the images demonstrate an aligned arrangement after 3 days on the hMSCs cell sheet (D). White arrows indicate intracellular vacuoles formation (Scale bar= 100 μm).

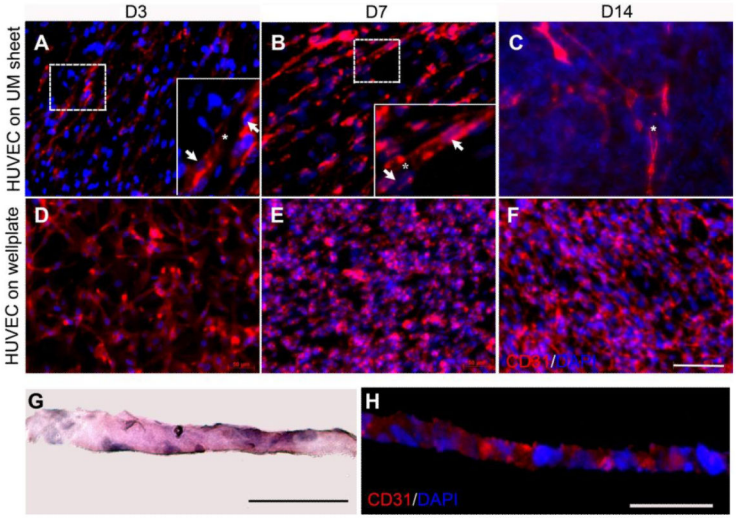

Fig. 3.

Immunofluorescent staining images of CD31 indicated a progressive process of lumen formation when HUVECs were cultured on the hMSCs sheet for 3, 7, and 14 days (A-C), and fluorescent image of HUVECs cultured on the well-plate for 3, 7, and 14 days (D-F). H&E staining (G) and immunofluorescent staining (H) were performed on each cross-section. HUVECs were seeded on the hMSCs sheet and observed for 7 days. White arrow indicates nuclei, asterisks indicate lumen formation. a-f: Scale bar= 100 μm. G-H: Scale bar= 50 μm.

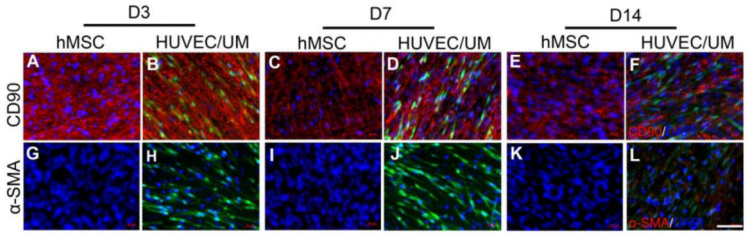

Fig. 4.

Immunofluorescent staining images of hMSCs sheet with CD90 on day 3, 7, and 14 (A,C,E), and hMSCs sheet with HUVECs seeded (B,D,F). Fluorescent image of α-SMA when hMSCs sheet was continuously cultured for 3, 7, and 14 days (G,I,K), and when HUVECs were cultured on the hMSCs sheet (H,J,L). Red: CD90 and α-SMA; Blue: DAPI. Green: HUVEC. Scale bar= 100 μm.

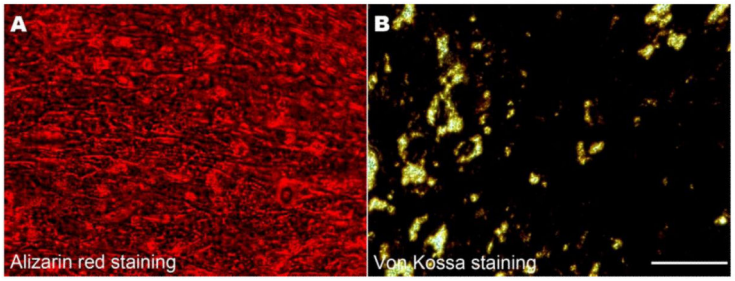

Fig. 5.

Alizarin red staining (A) and Von Kossa staining (B) images indicated a large number of calcium nodes (A: red) and calcium matrix deposition (B: black) after 21 days incubation (Scale bar= 100 μm).

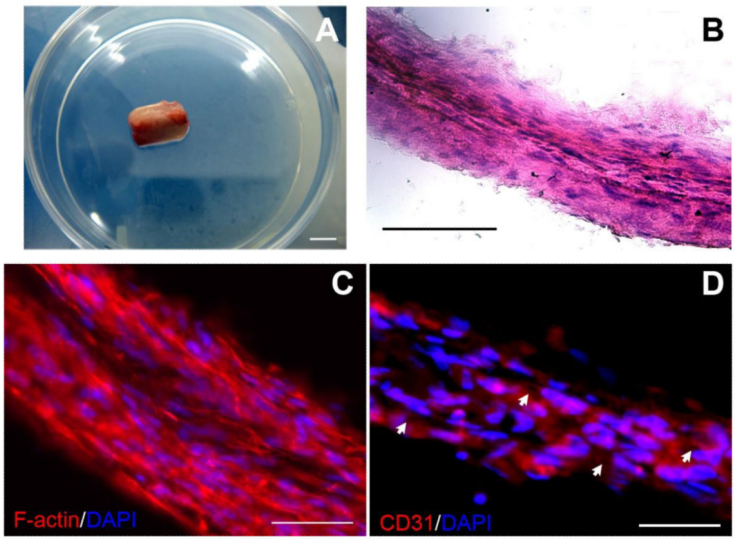

Fig. 6.

A gross view display of the composite cell sheets on a silicone rubber cylinder (A) (Scale bar= 1 mm). H&E staining showed the composite structure layers sheets (B) (Scale bar= 100 μm). F-actin staining indicated that the cells between two layers could grow together to connect with each other (C). Immunofluorescent staining for CD31 showed that lumen structures appeared among the multilayered constructs (D) (Scale bar= 50 μm).

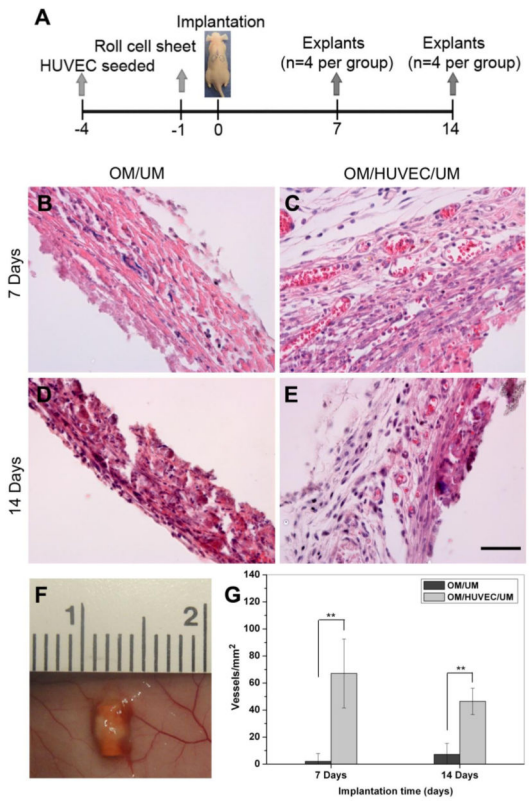

Fig. 7.

H&E staining of removed implants *in vivo*. Schematic figure shows the timeline of implantation: the constructs with HUVECs named OM/HUVEC/UM as experiment group, and a same rolled cell sheet constructs without HUVECs named OM/UM as a control. The implants were retrieved after 7 and 14 days *in vivo* (A). Representative images of H&E-stained sections from OM/HUVEC/UM and OM/UM implants, revealing the presence of numerous blood vessels containing murine erythrocytes (B-E). The overall view of a representative implant under skin is shown in (F). The extent of the vascular-network formation was quantified by measuring the microvessel density (G). The data are presented as mean ± SD. Significant difference between the OM/HUVEC/UM and OM/UM are shown as ** (**$p<0.01$, n=8) (Scale bar= 50 μm).

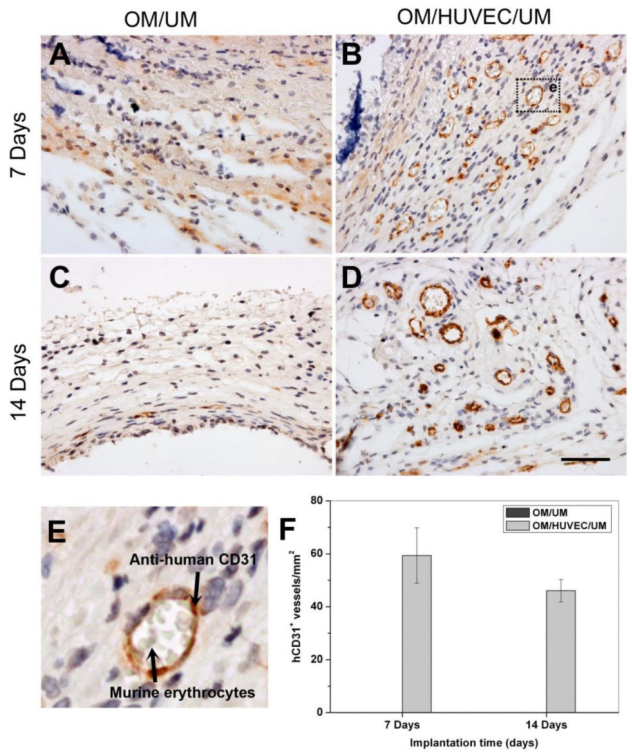

Fig. 8.

Immunohistochemistry staining images of CD31 for implants *in vivo*. Images of the engineered microvessels stained positive for human CD31, murine erythrocytes infiltrated into the lumen, which indicated the formation of functional blood vessels (A-D). A local magnification of a lumen containing murine erythrocytes is shown in (E). The percentage of human-CD31-expressing blood vessels (n=8) (F) (Scale bar= 50 μm).

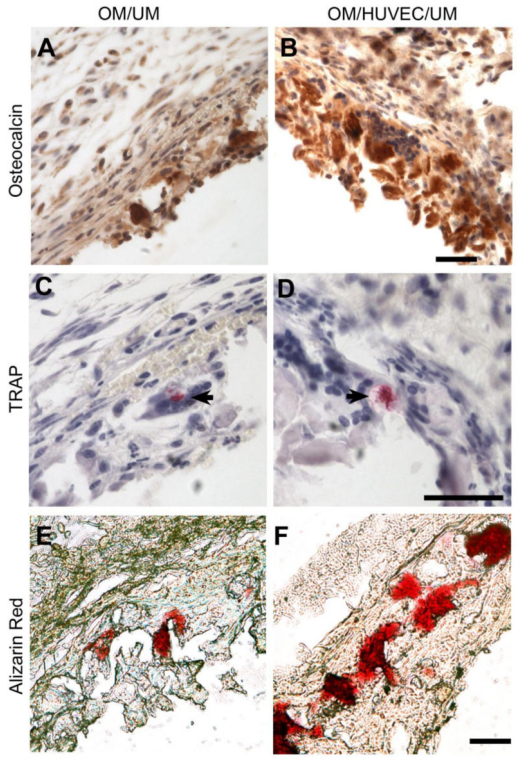

Fig. 9.

Immunohistochemistry staining images of osteocalcin for OM/UM (A) and OM/HUVEC/UM constructs (B). Osteoclast activity is shown through TRAP staining for in OM/UM (C) and OM/HUVEC/UM constructs (D) (black arrow). Alizarin red staining for mineralized calcium nodes in OM/UM (E) and OM/HUVEC/UM constructs (F) (Scale bar= 50 μm).